Insight into the ionotropic gelation of chitosan using tripolyphosphate and pyrophosphate as cross-linkers

Pasquale Sacco[a,*], Sergio Paoletti[a], Michela Cok[a], Fioretta Asaro[b], Michela Abrami[c], Mario Grassi[d], Ivan Donati[a]

[a] Department of Life Sciences, University of Trieste, Via Licio Giorgieri 5, I-34127 Trieste, Italy
[b] Department of Chemical and Pharmaceutical Sciences, University of Trieste, Via Licio Giorgieri 1, I-34127 Trieste, Italy
[c] Department of Life Sciences, Cattinara University Hospital, University of Trieste, Strada di Fiume 447, I-34149 Trieste, Italy
[d] Department of Engineering and Architecture, University of Trieste, Via Alfonso Valerio, 6/A I-34127 Trieste, Italy

ARTICLE INFO

Accepted 14 July 2016

Keywords:
Ionotropic gelation
Chitosan hydrogel
Tripolyphosphate/pyrophosphate

ABSTRACT

Ionotropic gelation of chitosan by means of opposite charged ions represents an efficient alternative to covalent reticulation because of milder condition of use and, in general, higher biocompatibility of the resulting systems. In this work 90° light scattering (turbidimetry), circular dichroism (CD) and ^{1}H NMR measurements have been performed to study the interactions between the biopolymer and ionic cross-linkers tripolyphosphate (TPP) and pyrophosphate (PPi) in dilute solutions. Thereafter, a dialysis-based technique was exploited to fabricate tridimensional chitosan hydrogels based on both polyanions. Resulting matrices showed a different mechanical behavior because of their peculiar mesh-texture at micro/nano-scale: in the present contribution we demonstrate that TPP and PPi favor the formation of homogeneous and inhomogeneous systems, respectively. The different texture of networks could be exploited in future for the preparation of systems for the controlled release of molecules.

1. Introduction

Ionotropic gelation of biopolymers has all along gained appeal due to its ability to favor the fabrication of biocompatible systems to be used in biomedical field. This method exploits the electrostatic interaction that occurs between polyions and oppositely charged specific cross-linkers under defined range(s) of concentration and/or pH. Ionic cross-linking requires mild conditions of use; however, fine control of the gelation rate is a challenging task, because of the very fast self-assembly between polymer and cross-linker.

Among various biopolymers amenable to ionic cross-linking, chitosan represents a noteworthy example [1]. This polymer is mostly obtained from the alkaline deacetylation of chitin, one of the most abundant natural polysaccharide on earth [2,3], but other sources can directly provide chitosan as such (*e.g.* yeasts). With respect to the parent polymer, chitosan is soluble in water under acidic condition thanks to the protonation of its amino groups (pKa values range from 6.2 to 7 depending on the type of chitosan and conditions of measurement) [2] by favoring the solvation of polymer chains. In these conditions, chitosan behaves as a polycation and, consequently, may favor electrostatic interactions.

On the other hand, tripolyphosphate (TPP) is by far the most employed cross-linker to ionically reticulate chitosan due to its high net negative charges (ranging from one to five depending on pH) per monomeric unit. For instance, TPP was successfully exploited to obtain chitosan nanoparticles and nano/micro-gels [4–7]. It has been demonstrated that the colloidal stability of these systems is deeply affected by many parameters like polymer and cross-linker concentration, pH, ionic strength, temperature and others [8]. In the recent years, the molecular interactions between chitosan and TPP have been investigated by several authors. For instance Koukaras et al. identified primary-interaction ionic cross-linking configurations defined as H-link, T-link, and M-link, and quantified the corresponding interaction energies [9]. Lapitsky et al. demonstrated the pivotal role of the monovalent salt sodium chloride (NaCl) to weaken and to slow down the otherwise too strong polycation-TPP interactions, thus ensuring the colloidal stability of resulting micro-gels [7,10]. Moreover, they also proved that not only TPP but also pyrophosphate (PPi) was able to boost the ionotropic gelation of chitosan to the extent of obtaining stable suspensions of nanoparticles [11,12]. On the other hand, Shu and Zhu used both polyanions to cross-link chitosan films upon soaking in TPP/PPi solutions [13].

* Corresponding author.
E-mail address: psacco@units.it (P. Sacco).

Although much work has been done by evaluating such interactions in dilute solutions, the formation of macroscopic hydrogels chitosan-based was by far less investigated with respect to negatively charged polysaccharides, *e.g.* alginate. An interesting attempt was provide by Khong et al. who mixed at a pH of about 7 an intermediate acetylated chitosan ($F_A = 0.4$) with mannuronate oligomers and subsequently lowered the pH by using GDL, thus ensuring the protonation of chitosan and the consequent interactions with oligomers [14]. Simultaneously, in our previous contributions a dialysis-based technique (named "slow ion diffusion technique") was devised, which proved to control the ionotropic gelation of a confined chitosan solution enabling the fabrication of cylindrical hydrogels and dried membranes for biomedical application purposes [15,16].

In the first part of the present contribution the investigation upon TPP-chitosan interactions in dilute solutions is reported. A comparison with PPi is presented in order to spot the different contribution of polyanions to polymer binding. Switching from dilute to concentrated solutions, the rationale for the second part of work is to study the different contribution of the two cross-linkers to the formation of chitosan-based hydrogels obtained by means of the slow ion diffusion technique. To the best of our knowledge, in this work we report for the first time the ability of the less popular cross-binder PPi giving rise to the formation of cylindrical macroscopic networks, distinguished by lower mechanical properties and with an inhomogeneous polymer profile with respect to TPP-hydrogels.

2. Materials and methods

2.1. Materials

Medium molecular weight chitosan (fraction of acetylated units, $F_A = 0.23$ determined by ^{1}H NMR), was purchased from Sigma-Aldrich and purified by precipitation with isopropanol, followed by a dialysis against deionized water. The molecular weight of chitosan was determined by viscosity measurements (see below). Sodium perchlorate was from Carlo Erba, Italy. Sodium tripolyphosphate pentabasic – $Na_5P_3O_{10}$ – (TPP ≥ 98.0%), sodium pyrophosphate tetrabasic – $Na_4P_2O_7$ – (PPi ≥ 95%), sodium chloride and glycerol (*ReagentPlus*® ≥99.0%) were all purchased from Sigma-Aldrich Chemical Co.

2.2. Viscosity measurements

The intrinsic viscosity [η] of chitosan was measured at 25 °C by means of a Schott-GeräteAVS/G automatic measuring apparatus and a Schott capillary viscometer. Chitosan was solubilized in deionized water (final concentration = 2 g L^{-1}) and pH was adjusted to 4.5 by HCl 0.5 M. After overnight stirring, an equal volume of buffer AcOH/AcNa (40 mM) – NaCl (0.2 M), pH = 4.5, was added. The polymer was filtered through 0.45 μm Millipore filters prior the measurements. Intrinsic viscosity was calculated by analyzing the polymer concentration dependence of the reduced specific viscosity η_{sp}/c and of the reduced logarithm of the relative viscosity $\ln(\eta_{rel})/c$ by use of the Huggins (Eq. (1)) and Kraemer (Eq. (2)) equations, respectively:

$$\frac{\eta_{sp}}{c} = [\eta] + k[\eta]^2 c \quad (1)$$

$$\frac{\ln \eta_{rel}}{c} = [\eta] - k'[\eta]^2 c \quad (2)$$

where k and k' are the Huggins and Kraemer constants, respectively. The intrinsic viscosity values were averaged and the resulting [η] was found to be 836 mL g^{-1}. The molecular weight of chitosan was calculated in agreement to the Mark-Houwink equation reported in Berth *et al.* [17] and it was found to be 270000.

2.3. Light scattering (Turbidimetry)

A Perkin-Elmer LS50 B spectrofluorimeter was used to record the intensity of the light scattered (90°) by dilute chitosan solutions (0.05% w/v and 2 mL as final volume), upon irradiation with a 550 nm incident light ($T = 25$ °C). Chitosan was solubilized in acidified deionized water (pH = 2.6) and resulting solutions were titrated using either TPP or PPi solutions (6 μL injections) to gradually increase the molar ratio (r) between the cross-linker and the monomeric unit of chitosan ($r = [\text{crosslinker}]/[\text{monomeric unit}]_{ru}$). Each injection increased r by 0.02 units. Before analysis, solutions were allowed to equilibrate for one minute. Considering the contribution of *N*-acetylglucosamine unit, the molecular mass of chitosan monomeric unit resulted 171 g mol^{-1}.

2.4. Circular dichroism (CD)

CD spectra of dilute chitosan solutions (0.05% w/v) were recorded in acidified deionized water (pH = 2.6) with a Jasco J-700 spectropolarimeter. The chitosan solution was titrated using either TPP or PPi solutions (3 μL injections) to gradually increase r. Each injection increased r by 0.02 units. For all measurements, the volume of each injection was considered negligible with respect to that of chitosan solution (1 mL): in fact, the volume increase (*i.e.* chitosan dilution) was about 13% at $r = 1$, while r never exceeded 0.24, corresponding to a dilution of less than 4%. Before analysis, solutions were allowed to equilibrate for one minute. Ellipticity of titrated solutions (θ_r) was normalized by that of chitosan (θ), with no correction for dilution. Data are expressed as values of reduced specific ellipticity in agreement to the equation

$$\Delta\theta = (\theta_r - \theta)/|\theta|$$

A quartz cell of 1 cm optical path length was used, always using the following setup: bandwidth 1 nm, time constant 2 s, scan rate 20 nm min^{-1}, wavelength range 250–208 nm. Three spectra were averaged for each measurement.

2.5. Nuclear magnetic resonance (^{1}NMR)

^{1}H NMR analyses were performed on chitosan solutions (0.2% w/v in 0.2 M acetic acid as a solvent, pH = 2.6), with addition of TPP or PPi with final value $r = 0.16$. The ^{1}H NMR spectra were recorded at 25 °C, on a Varian VNMRS (11.74 T) NMR spectrometer operating at 499.65 MHz for proton. Water suppression was accomplished by means of WET [18]. A total of 512 scans were accumulated with a spectral width of 6 kHz over 16384 complex data points. The data were multiplied by a decaying exponential function (broadening factor 0.5 Hz) and zero filled twice prior to Fourier transform. The chemical shifts are referred to the chemical shift of the proton of HOD at 4.645 ppm.

2.6. Chitosan hydrogels preparation

Wall-to-wall hydrogels were obtained by a slow diffusion technique [15]. Briefly, a solution composed by chitosan (3% w/v) and glycerol (5% v/v) was casted into a mold (diameter = 22 mm, thickness = 2.5 mm) closed by two dialysis membranes (average flat width 33 mm, Sigma Aldrich, Chemical Co.) and fixed by double circular stainless iron rings. The system was hermetically sealed and immersed into a gelling solution (final volume 50 mL) containing anions (TPP or PPi) – NaCl (150 mM) – glycerol (5% v/v). TPP and PPi concentrations were varied so that r spanned in the range from 0.3 to 7. Ion diffusion proceeded for 24 h under moderate stirring at room temperature allowing hydrogel formation.

2.7. Mechanical spectroscopy

Rheological characterization of TPP/PPi chitosan hydrogels was performed by means of a controlled stress rheometer Haake RheoStress RS150 operating at 25 °C using a shagreened plate apparatus (HPP20 profiliert: diameter = 20 mm) as the measuring device. To avoid water evaporation from the hydrogel, measurements were performed in a water-saturated environment formed by using a glass bell (solvent trap) containing a wet cloth. In addition, to prevent both wall-slippage [19] and excessive gel squeezing, the gap between plates was adjusted, for each sample, by executing a series of short stress sweep tests ($\nu = 1$ Hz; stress range 1–5 Pa) characterized by a reducing gap [20]. The selected gap was that maximizing the value of the elastic modulus G' (used gaps ranged between 2.5 and 2.0 mm). For each hydrogel, the linear viscoelastic range was determined by means of a stress sweep test consisting in measuring elastic (G') and viscous (G″) moduli variation with increasing shear stress ($1\,\text{Pa} < \tau < 5\,\text{Pa}$) at a frequency $\nu = 1$ Hz (hence with $\omega = 2\pi\nu = 6.28\,\text{rad}\,\text{s}^{-1}$). The mechanical spectrum of hydrogels was determined by measuring the dependence of the elastic (G′) and viscous (G″) moduli from the pulsation ω at constant shear stress $\tau = 5$ Pa (well within the linear viscoelastic range which, for all samples, spans up to at least 30 Pa).

2.8. Evaluation of homogeneity

The homogeneity of the TPP and PPi hydrogels was assessed by means of the method reported elsewhere [21]. Briefly, cylindrical hydrogels were cut perpendicular to the cylinder axis into five slices with roughly the same thickness (5 mm). Only for these studies, the controlled gelation of chitosan was reached by exploiting a dialysis tube (diameter 25 mm) flooded into the same gelling solution mixture described in paragraph 2.6. After measuring their wet weights by an analytical balance, the slices were dried at 40 °C for 24 h. Samples were weighed again after drying, and their dry/wet weight ratios (D_w/W_w) were calculated.

2.9. Image analyses

Image analyses were carried out on TPP and PPi hydrogels cross-sections. Hydrogel slices of approximately 1 mm of thickness were dried in ethanol 70% v/v and overnight contrasted using $UO_2(CH_3COO)_2$ 0.2% w/v. Subsequently slices were totally dried in ethanol 100% v/v and finally embedded in Epoxy resin after completely removing the alcohol. Ultrathin sections were cut by means of a microtome (equipped with a diamond blade) and gently deposited onto Nickel grids. Visual analysis and image record were performed using a PHILIPS EM Transmission Electron Microscope.

3. Results and discussion

3.1. Interaction between chitosan and cross-linkers in dilute solution

Any interaction of a cross-linker with a polymer to produce colloidal complexes (up to gels) will start with chain–chain association, paralleled by an increase of the molar mass (and of the dimensions) of the polymeric species. For this reason, scattering techniques probably rank first among the methods which can be employed to monitor such association behavior. The relative intensity (90°) of chitosan solutions in water upon addition of TPP and of PPi is reported in Fig. 1 as a function of the molar ratio, *r*, between the cross-linker and monomeric unit of chitosan. In agreement with published data obtained by dynamic light scattering analyses using a different type of chitosan (lower Mw and F_A) [11], the addition of TPP is immediately accompanied by an increase of the scattering

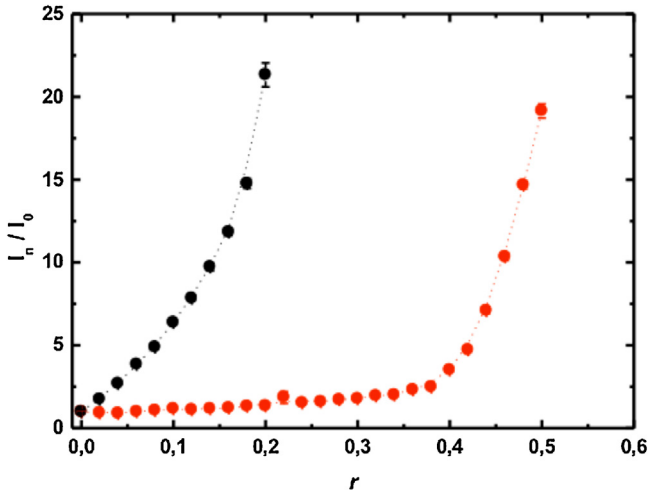

Fig. 1. 90° scattered light for chitosan solutions titrated either with TPP (black dots) or PPi (red dots). The total polymer concentration was 0.05% w/v in all of the cases analyzed. Data are expressed as the ratio between the intensity of titrated solutions (I_n) and the intensity of that of chitosan alone (I_0) *vs.* the molar ratio between cross-linker and monomeric unit of chitosan (*r*). Values are reported as mean (±SD, $n = 8$). Dotted curves are drawn to guide the eye. (For interpretation of the references to colour in this figure legend, the reader is referred to the web version of this article).

(up to the maximum measurable value), whereas in the case of PPi only a moderate, albeit non negligible, increase is observed up to about $r = 0.4$, followed by an abrupt increase of the observed scattering up to the (experimental limiting) value of about $r = 0.5$. For both TPP and PPi, at the highest accessible *r* value the solution becomes clearly turbid, thus indicating the formation of visible coacervates. Turbidimetry analyses clearly demonstrated the higher binding affinity of TPP with respect to PPi for the chitosan chains. This may be ascribed to the presence of an extra negative charge in the case of TPP. Indeed, at the pH value here investigated, TPP and PPi should bear almost three and two negative charges, respectively, one on each monophosphate unit.

In general, in the case of counterion-induced association of ionic polysaccharides, the association process is the result of a conformational change of the polysaccharide chain, which assumes a well-defined, ordered conformation as a prerequisite of chain alignment (and ion binding) and junction formation [22,23]. Circular dichroism is a versatile technique already employed in the study of polysaccharides and their mixtures [24,25]. It is notably sensitive to macromolecule conformational variations, so one expects CD could be an useful method to investigate upon polymer/cross-linker interactions. Since chitosan is a chiral molecule presenting the *N*-acetylglucosamine chromophore group which absorbs radiation in the range of 200 − 250 nm, it is possible to record its CD spectrum. Fig. 2A reports the CD spectrum of a 0.05% w/v chitosan solution showing the presence of a negative minimum at ~210 nm referring to the UV-absorption (stemming from the $n \rightarrow \pi^*$ transition) of the *N*-acetilglucosamine unit [24]. Titration of the chitosan solution by means of either TPP or PPi solutions was performed by gradually increasing the molar ratio *r* between cross-linker and the repeating unit of chitosan. It is noteworthy underlining that titration was carried out up to the experimental limit of the setup sensitivity. In the case of TPP, this limit was accompanied by turbidity appearance (due to the formation of visible coacervates). Indeed, beyond this limit the spectroscopic signal variation cannot be any longer associated to changes in chromophore dissymmetry but, rather, to changes in the scattered light due to the presence of micro-aggregates. Fig. 2B shows the variation of chitosan ellipticity following titration with both cross-linkers. The experimental CD data have been reported as the ratio of the (relative) difference of

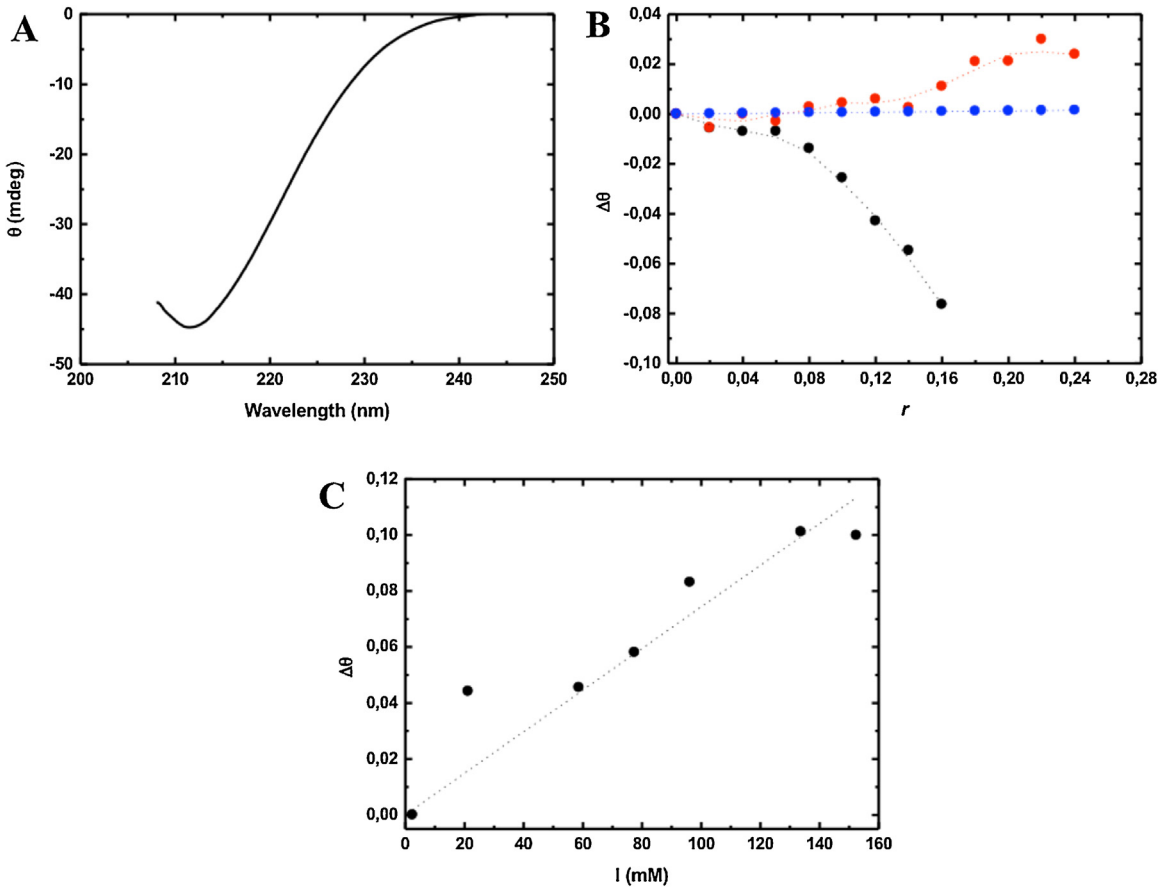

Fig. 2. (A) CD curve of the chitosan solution (0.05% w/v) in acidified deionized water (pH = 2.6). (B) Variation of reduced ellipticity by consecutively titrating previous polymer solution by means of either TPP (black dots) or PPi (red dots); blue dots represent the variation of reduced ellipticity due to the ionic strength determined by the PPi anions; dotted curves are drawn to guide the eye. (C) Variation of reduced ellipticity for chitosan solutions with constant polymer concentration 0.05% w/v and different ionic strength, I, due to the presence of $NaClO_4$, pH = 2.6; dotted line represents the best linear fitting among experimental points (For interpretation of the references to colour in this figure legend, the reader is referred to the web version of this article).($\Delta\theta \alpha 7 \cdot 10^{-4} I$)

ellipticity between the titrated solutions and the cross-linker-free polymer solution, here defined as $\Delta\theta$.

In the case of TPP, all observed variations are negative, and the shape of the CD curve *vs.* *r* closely parallels that of the scattering intensity (cfr. Fig. 1), suggesting that the two processes are simultaneous. To ensure that the small, albeit well detectable, relative CD change (at most 8% of the original value) did not stem from artifacts deriving from the formation of chiral aggregates [26], the position of the cuvette along the optical path was changed with respect to the detector. Even at the highest *r* value investigated, no change in the measured ellipticity was observed, thus confirming the molecular origin of the observed variation. To ascertain whether the observed $\Delta\theta$ stems from a specific TPP/chitosan interaction or from a non-specific electrostatic effect caused by the change in the solution ionic strength (I) brought about by the multivalent anion, $\Delta\theta$ was measured for chitosan solutions (at constant polymer concentration = 0.05% w/v) increasing I from zero to 150 mM by $NaClO_4$. The results are reported in Fig. 2C: they indicate that a positive $\Delta\theta$ is brought about by an increase of I. However, the calculated effect due to change of ionic strength in the *r* domain of the significant variations induced by TPP is totally negligible (not shown), thus pointing to a specific effect of the multivalent species on the chitosan chain. Unfortunately, upon exceeding *r* = 0.16, the solution became gradually turbid for the formation of coacervates, thus preventing from obtaining more data that would have allowed for clearly establishing the presence of a cooperative binding between chitosan and the anions. The latter interpretation was suggested by Huang et al. in the same range of *r* based on ITC studies which accompanied DLS investigation, where "the cooperative increase in the exothermic binding enthalpy was evident from the very beginning of the titration" [11].

On the other hand, when using PPi as anion for the titration of chitosan solution, the relative increase of the CD change was much lower than in the case of TPP, but opposite in sign (at least for $r > 0.15$), where the $\Delta\theta$ became slightly larger than experimental uncertainty (Fig. 2B). Also in this case, the observed $\Delta\theta$ effect in the higher range of *r* is by far larger than that induced by I alone. The interesting observation is that the experimental $\Delta\theta$ data are different for the two multivalent species, that of TPP being surprisingly different from that of PPi (specific) and of I (unspecific). Whether such $\Delta\theta$ difference corresponds to a well-defined difference in conformation brought about by the two anions (and I) cannot be stated on the basis of the present results and only a suggestion for further investigation can be set forth. The outcome is anyway in line with ITC investigations where an enthalpy reduction from −6 to −1 kJ mol^{-1} was observed for dilute chitosan solutions upon PPi addition for the same range of molar ratios, so as to confirm molecular interactions between the polymer and the cross-linker [11].

To further focus into the behavior of chitosan upon binding with both oligo-anions, ^{1}H NMR measurements were performed and the results are pointed out in Fig. 3. A molar ratio *r* of 0.16 was chosen for comparison purposes. The glucosamine H2 proton, which is sensitive to pH changes [27], is unaffected by the small addition of

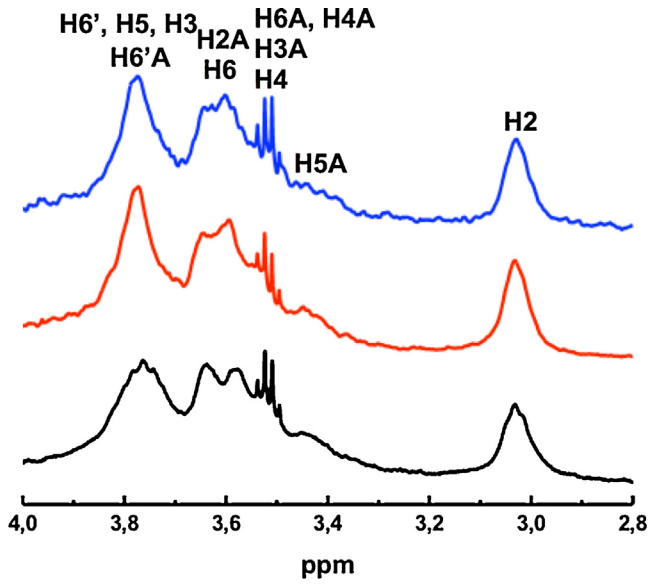

Fig. 3. ^{1}H resonances in the 4–2.8 ppm spectrum region for chitosan (black solid line), chitosan + PPi (red solid line) and chitosan + TPP (blue solid line) with cross-linker/chitosan monomeric unit ratio (r) of 0.16 in 0.2 M CH_3COOH solution (pH = 2.6). The assignments for glucosamine and *N*-acetylglucosamine protons (labelled as A) are reported. (For interpretation of the references to colour in this figure legend, the reader is referred to the web version of this article).

either TPP or PPi, ruling out the deprotonation as the origin of the conformational changes detected by light scattering and CD, which therefore should be attributed to specific interactions of chitosan with multivalent anions. Rather, the presence of TPP and PPi affects the pattern of the envelope of the overlapped resonances of most protons of chitosan monomeric units, between 3.9 and 3.5 ppm, in agreement with the occurrence of chain reconfiguration. Hence, a probable explanation of the light scattering, CD and ^{1}H NMR observations is that a gradual neutralization of chitosan charges occurs with strong interactions with polyphosphate anions, as already demonstrated by means of Z-potential measurements [7], consequently bringing about a conformational rearrangement of polymer chains.

3.2. Tridimensional chitosan hydrogels reticulated by TPP and PPi

In our previous paper we already demonstrated the fine control on the ionotropic gelation of confined chitosan when dialyzed against a TPP solution [15]. The second aim for the present work was to explore the ability of PPi to form tridimensional matrices by exploiting the slow ion diffusion technique and, consequently, to study the different mechanical behavior or the resulting networks. In order to achieve this purpose, chitosan concentration was kept constant (3% w/v) in the vessel and different cross-linker concentrations were selected so as to vary r. For both anions, no hydrogel formation occurred for $r < 3.1$. Upon exceeding this limit the formation of macroscopic systems by both cross-linkers took place.

When the dialysis starts, TPP or PPi migrate through the semipermeable membrane and bind to positively charged chitosan: the ionotropic gelation takes place and the confined viscous chitosan solution tends to gradually become opaque. This phenomenon is due to the self-assembly process between chitosan and cross-linkers, as already reported in literature, which proceeds through a two-step process: (*i*) the formation of small primary complexes and (*ii*) their subsequent aggregation into larger, higher-order colloids, *i.e.* coacervates (microgels) [10]. It is noteworthy to point out the analogy with the formation of

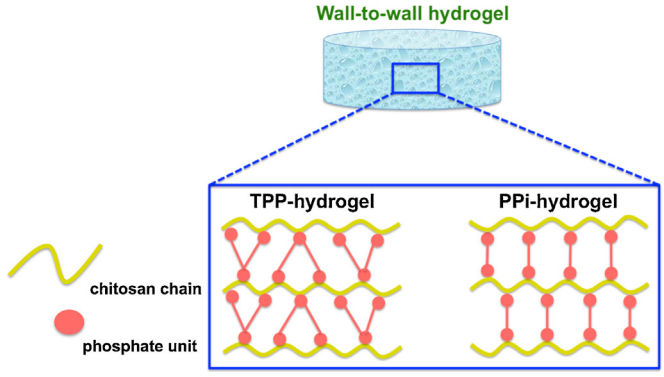

Fig. 4. Wall-to-wall hydrogel chitosan-based obtained by slow ion diffusion technique. The inset represents the hypothetical disposition of junctions within the hydrogel where polymer chains (yellow ribbons) bind either TPP or PPi by electrostatic interactions. Cross-linkers are represented as reddish dots where each one may be considered as a single phosphate unit or a single negative charge. (For interpretation of the references to colour in this figure legend, the reader is referred to the web version of this article).

silica nanoparticles under basic catalysis originated by a similar procedure [28]. Another example is reported by the formation of macroscopic coacervate droplets by poly(allylamine hydrochloride)/citrate complexes [29]. Nevertheless, in our system we have to consider an additional step (*iii*), that is the aggregation of coacervates so as to obtain a 3D macroscopic network (Fig. 4). The slow diffusion of both TPP and PPi through dialysis membranes, assisted by the screening effect of the supporting salt (NaCl) and by van der Waals interactions between polymer chains, enables to finely control the self-assembling of microgels until an opaque wall-to-wall system is obtained.

In order to investigate the different mechanical behavior of the resulting hydrogels, rheological measurements were performed. Frequency sweep analyses were carried out to record mechanical spectra of hydrogels (Fig. 5). Experimental measurements were fitted by means of the Maxwell model described elsewhere [30]. The number of Maxwell elements (sketched by a sequence of elastic springs, of constant G_i, and viscous dashpot elements) was selected through a statistical procedure to minimize the product $\left(\chi^2 \cdot n\right)$, where χ^2 is the sum of the squared errors while n is the number of fitting parameters. Mechanical spectra in Fig. 5A-B, point out that both storage (G′) and loss moduli (G″) differ by approximately one order of magnitude for almost two decades of frequency, thus indicating the "strong" nature of TPP/PPi hydrogels. By means of Maxwell model the shear modulus (G) can be calculated as:

$$G = G_e + \sum_{i=1}^{n} G_i$$

where G_e is the spring constant of the purely elastic Maxwell element whereas G_i refers to the spring constant of the other Maxwell elements. Shear modulus is a pivotal parameter to assess the stiffness of a material. In general terms, it has been found that shear moduli of TPP-containing hydrogels were higher than those prepared using PPi. More in detail, in the case of TPP hydrogels the shear modulus at $r = 3.8$ was higher than that with $r = 7.0$ (Fig. 5C). The best mechanical response to the shear stress was observed for hydrogels with $r = 5.2$. The shear modulus trend for present TPP hydrogels was in line with that already demonstrated for systems obtained with a different TPP powder (technical grade 85%) and higher molecular weight chitosan [15]. Moreover, a similar behavior was identified for the purely elastic constant G_e. In the case of PPi hydrogels, shear modulus was found to increase with the increasing of r as pointed out in Fig. 5D. In any case, shear moduli of TPP hydrogels (except for $r = 7.0$) were higher than those of PPi hydrogels, thus indicating higher stiffness for the first.

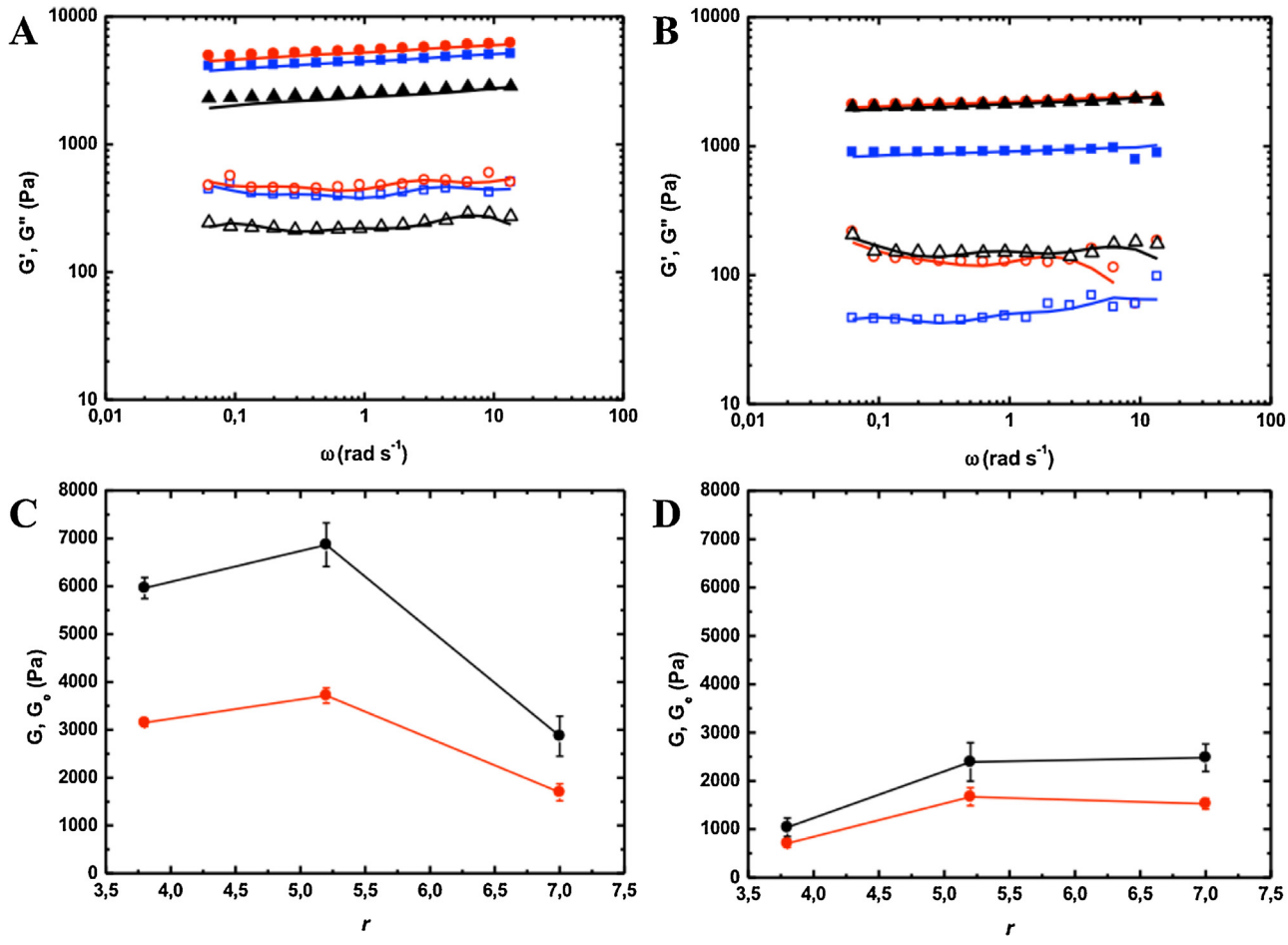

Fig. 5. Upper plots. G′ (full symbols) and G″ (open symbols) for chitosan-TPP (A) and chitosan-PPi (B) hydrogels at different cross-linker/chitosan monomeric unit molar ratios (r) of 3.8 (blue squares), 5.2 (red circles) and 7.0 (black triangles); solid lines represent the best fitting by means of Maxwell model. Lower plots. Dependence of the shear modulus (±SD), black solid line, and G_e (±SD), red solid line, *vs.* different r for chitosan-TPP (C) and chitosan-PPi (D) hydrogels. (For interpretation of the references to colour in this figure legend, the reader is referred to the web version of this article).

The number of moles of point-like junctions (polymeric network crosslink density, ρ) between chitosan chains per hydrogel unit volume can be calculated by exploiting the Flory's theory in agreement to the equation:

$$\rho = \frac{G}{RT}$$

where R is the universal gas constant, T is the temperature and G is the shear modulus. By assuming the parameter ξ as the diameter of the collection of spheres that composes an ideal network with a regular mesh (equivalent network theory), cross-link density enables to easily calculate the average network mesh size as

$$\xi = \sqrt[3]{\frac{6}{\pi \rho N_a}}$$

where N_a is the Avogadro number [31]. The results for both TPP and PPi hydrogels with different amount of cross-linker are reported in Table 1.

Scrutiny of the results of Table 1 seems to suggest a peculiar comparative behavior of the two systems. In the case of TPP, a higher cross-link density (and consequently a smaller mesh size) is observed for $r = 5.2$. ρ very slightly decreases upon decreasing r (with a negligible increasing of ξ); however, an increase of r (to 7.0), seems to be detrimental for the mechanical performance of the hydrogels (G reduces to less than half of the value at $r = 5.2$), with a parallel drop of ρ and an upraise of ξ. The drop of mechanical performance following to the increase of cross-linker is not unusual for biopolymer-based hydrogels. For instance, it was already demonstrated that the increasing of calcium carbonate, beyond a critical limit, caused the Young's modulus drop in cylindrical alginate hydrogels [32]. On the contrary, the effect of the increase of cross-linker in the case of PPi seems to be more monotonic in trend, but with an effect which is always beneficial. Interestingly, the ratio of the G values of TPP and PPi is about 6 at $r = 3.8$, but it drops to about 1.2 at $r = 7.0$. Correspondingly, the ratio of ρ values passes from about 8 to about 1.2, and that of the average network mesh size from 0.5 to about 1.

The polymer mesh distribution within hydrogels was studied qualitatively by means of TEM analyses. By comparing TPP-hydrogels to PPi-ones (Fig. 6A and B, respectively) the different cross-linking density is shown. At a glance, randomly distributed networks composed of entangled polymer (dark ribbons) and not-contrasted zones (grey spaces) can be observed. TEM image of TPP-hydrogels (Fig. 6A) displays a homogeneous distribution of chitosan both with a wide range of pore sizes and with generally lack of aggregates. On the contrary, PPi-hydrogels show a not-homogeneous network characterized by a reduction of point-by-point connectivity. The results are consistent with other physical-gels (pectin and alginate), where the random distribution of polymer chains was observed [33–35]. Furthermore, no preferential direction of chitosan chains was identified for both hydrogels, so as to rule out anisotropic effects on mechanical properties. The outcomes clearly demonstrated that, albeit no discrepancies at

Table 1
Physical-chemical parameters for TPP/PPi-containing hydrogels. *r* represents the molar ratio between the cross-linker and the monomeric unit of chitosan. Shear modulus (G), polymeric network crosslink density (ρ) and average network mesh size (ξ) were calculated by means of Maxwell model, Flory's and equivalent network theories, respectively.

	PPi			TPP		
r	3.8	5.2	7.0	3.8	5.2	7.0
G (kPa)	1.04 + 0.19	2.39 + 0.40	2.48 + 0.28	5.95 + 0.22	6.87 + 0.45	2.87 + 0.42
ρ x 10^{-6} (mol cm^{-3})	0.29 + 0.03	0.97 + 0.16	1.00 + 0.11	2.40 + 0.09	2.77 + 0.18	1.16 + 0.17
$\xi(nm)$	22.3 + 0.9	14.9 + 0.8	14.7 + 0.8	11.0 + 0.1	10.5 + 0.2	14.0 + 0.7

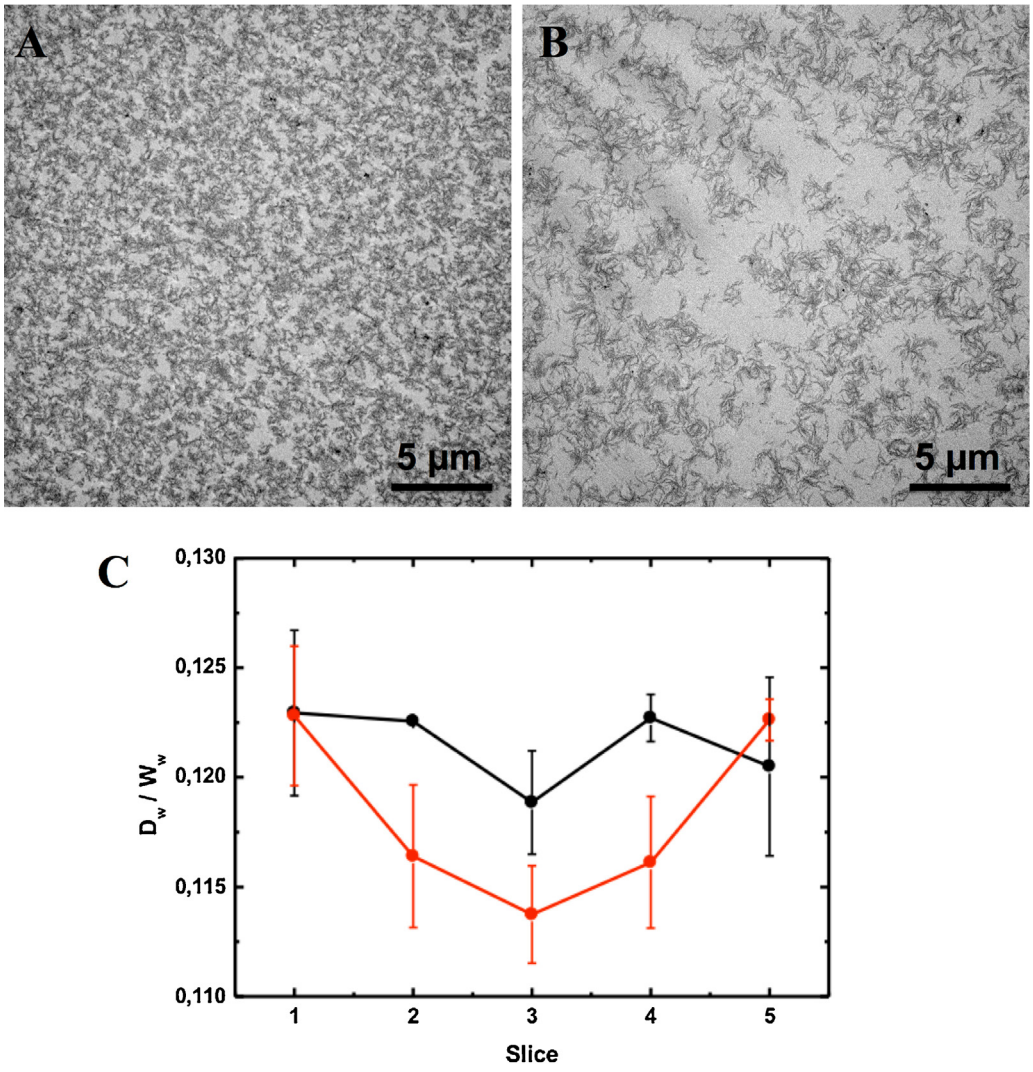

Fig. 6. Chitosan meshes distribution in TPP (A) and PPi (B) hydrogel cross-sections with cross-linker/chitosan monomeric unit molar ratio of 3.8. The polymer was contrasted by means of $UO_2(CH_3COO)_2$ 0.2% w/v. TEM images were acquired at a constant accelerating voltage of 100 kV. (C) Polymer distribution profile along chitosan-TPP (black solid line) and chitosan-PPi (red solid line) hydrogel cross-section expressed as dry/wet weight ratios of slices (numbered 1–5). Data are expressed as mean (±SD). (For interpretation of the references to colour in this figure legend, the reader is referred to the web version of this article).

the macroscopic level may be identified, the different reticulation throughout the network strictly affects the mechanical behavior of hydrogels.

To get further insights about the polymer network within chitosan hydrogels, the distribution of polysaccharide within systems was studied. By considering the very thin thickness of hydrogels fabricated with the standard method reported in paragraph 2.6, a slight modification of protocol was devised in order to increase the cross-section surface. To this purpose, a dialysis bag of 25 mm as diameter was used for the gelation process. Resulting hydrogels were cut along the gelation axis; the cross-linker/chitosan monomeric unit ratio of 3.8 was selected for the fabrication of hydrogels and the results are shown in Fig. 6C. Polymer distribution within TPP hydrogels demonstrated to be approximately constant along cylinder axis (homogeneous distribution), albeit with higher experimental error to the boundary. At variance, PPi hydrogels showed a not-homogeneous profile of chitosan. More in detail, the amount of polymer was higher at the boundary compared to that of the core. This condition can be ascribed to a partial inhomogeneity occurred during the ionotropic gelation, likely due to the milder ability of PPi to bind chitosan, leading to the formation of a more liquid-like core. Our data close parallel what

already known for alginate-Ca^{+2} gels, where the polymer distribution (homogeneity/inhomogeneity) of resulting systems fabricated in similar experimental conditions was tuned by varying some parameters, *i.e.* the presence of non-gelling cations [36]. As a consequence, mechanical properties of hydrogels reticulated with the same amount of either TPP or PPi are essentially dissimilar as reported in Table 1 with higher shear moduli for the former.

4. Conclusions

In the present contribution the binding of cross-linkers TPP and PPi to chitosan was studied by turbidimetry, circular dichroism and ^{1}H NMR. Scattering analyses demonstrated the higher ability of TPP to interact with the biopolymer whereas CD measurements suggest chain reconfiguration of chitosan following to the specific interaction with polyanions and not to the unspecific contribution of their ionic strength. In the second part of work, the ability of not-traditional cross-linker PPi giving rise to the formation, by means of a hypothesized three-step process, of macroscopic hydrogels with different homogeneity and mechanical properties, with respect to TPP-networks, was demonstrated. Considering the different mesh texture at nano/microscale, both types of hydrogels could be potentially used in biomedical field, *i.e.* for the different release of small molecules.

5. Notes

The authors disclose any actual or potential conflict of interest.

6. Author contributions

Conceived and designed the experiments: PS, SP, MG, ID. Performed the experiments: PS, FA, MC, MA. Analyzed the data: PS, SP, FA, ID. Wrote the paper: PS, SP, FA.

Acknowledgments

This study was supported by the Friuli-Venezia Giulia Regional Government (Project: "*Nuovi biomateriali per terapie innovative nel trattamento delle ferite difficili*"-LR 47/78). The financial support to P.S. (Ph.D. scholarship) by the Friuli-Venezia Giulia Regional Government and by the European Social Fund (S.H.A.R.M. project-Supporting human assets in research and mobility) is gratefully acknowledged. Miss Greta Galiussi and Dr. Davide Porrelli are thanked for their skillful assistance in the experimental part.

References

[1] J. Berger, M. Reist, J.M. Mayer, O. Felt, N.A. Peppas, R. Gurny, Structure and interactions in covalently and ionically crosslinked chitosan hydrogels for biomedical applications, Eur. J. Pharm. Biopharm. 57 (2004) 19–34.
[2] K.M. Vårum, O. Smidsrød, Structure-Property Relationship in Chitosans, In: Polysaccharides Struct. Divers. Funct. Versatility Second, CRC Press, 2004, pp. 625–642.
[3] J. Malmo, A. Sandvig, K.M. Vårum, S.P. Strand, Nanoparticle mediated P-glycoprotein silencing for improved drug delivery across the blood-brain barrier: a siRNA-chitosan approach, PLoS One 8 (2013) e54182.
[4] P. Calvo, C. Remuñán-López, J.L. Vila-Jato, M.J. Alonso, Novel hydrophilic chitosan-polyethylene oxide nanoparticles as protein carriers, J. Appl. Polym. Sci. 63 (1997) 125–132.
[5] R.A. Hashad, R.A.H. Ishak, S. Fahmy, S. Mansour, A.S. Geneidi, Chitosan-tripolyphosphate nanoparticles: optimization of formulation parameters for improving process yield at a novel pH using artificial neural networks, Int. J. Biol. Macromol. 86 (2016) 50–58.
[6] A. Rampino, M. Borgogna, P. Blasi, B. Bellich, A. Cesàro, Chitosan nanoparticles: preparation, size evolution and stability, Int. J. Pharm. 455 (2013) 219–228.
[7] Y. Huang, Y. Lapitsky, Monovalent salt enhances colloidal stability during the formation of chitosan/tripolyphosphate microgels, Langmuir 27 (2011) 10392–10399.
[8] W. Fan, W. Yan, Z. Xu, H. Ni, Formation mechanism of monodisperse, low molecular weight chitosan nanoparticles by ionic gelation technique, Colloids Surf. B: Biointerfaces 90 (2012) 21–27.
[9] E.N. Koukaras, S.A. Papadimitriou, D.N. Bikiaris, G.E. Froudakis, Insight on the formation of chitosan nanoparticles through ionotropic gelation with tripolyphosphate, Mol. Pharm. 9 (2012) 2856–2862.
[10] Y. Huang, Y. Lapitsky, Salt-assisted mechanistic analysis of chitosan/tripolyphosphate micro- and nanogel formation, Biomacromolecules 13 (2012) 3868–3876.
[11] Y. Huang, Y. Lapitsky, Determining the colloidal behavior of ionically cross-linked polyelectrolytes with isothermal titration calorimetry, J. Phys. Chem. B. 117 (2013) 9548–9557.
[12] Y. Cai, Y. Lapitsky, Formation and dissolution of chitosan/pyrophosphate nanoparticles: is the ionic crosslinking of chitosan reversible? Colloids Surf. B: Biointerfaces 115 (2014) 100–108.
[13] X. Shu, K. Zhu, The influence of multivalent phosphate structure on the properties of ionically cross-linked chitosan films for controlled drug release, Eur. J. Pharm. Biopharm. 54 (2002) 235–243.
[14] T.T. Khong, O.A. Aarstad, G. Skjåk-Bræk, K.I. Draget, K.M. Vårum, Gelling concept combining chitosan and alginate-proof of principle, Biomacromolecules 14 (2013) 2765–2771.
[15] P. Sacco, M. Borgogna, A. Travan, E. Marsich, S. Paoletti, F. Asaro, et al., Polysaccharide-based networks from homogeneous chitosan-tripolyphosphate hydrogels: synthesis and characterization, Biomacromolecules 15 (2014) 3396–3405.
[16] P. Sacco, A. Travan, M. Borgogna, S. Paoletti, E. Marsich, Silver-containing antimicrobial membrane based on chitosan-TPP hydrogel for the treatment of wounds, J. Mater. Sci. Mater. Med. 26 (2015) 128.
[17] G. Berth, H. Dautzenberg, The degree of acetylation of chitosans and its effect on the chain conformation in aqueous solution, Carbohydr. Polym. 47 (2002) 39–51.
[18] G. Zheng, W.S. Price, Solvent signal suppression in NMR, Prog. Nucl. Magn. Reson. Spectrosc. 56 (2010) 267–288.
[19] R. Lapasin, S. Pricl, Rheology of industrial polysaccharides: theory and applications, Chapman and Hall: London, (1995); p 620.
[20] T.K.L. Meyvis, S.C. De Smedt, J. Demeester, W.E. Hennink, Rheological monitoring of long-term degrading polymer hydrogels, J. Rheol. (N. Y. N. Y.) 43 (1999) 933.
[21] C.K. Kuo, P.X. Ma, Ionically crosslinked alginate hydrogels as scaffolds for tissue engineering: part 1. Structure, gelation rate and mechanical properties, Biomaterials 22 (2001) 511–521.
[22] E.R. Morris, D.A. Rees, D. Thom, Characterisation of alginate composition and block-structure by circular dichroism, Carbohydr. Res. 81 (1980) 305–314.
[23] I. Donati, J.C. Benegas, A. Cesàro, S. Paoletti, Specific interactions versus counterion condensation 2. Theoretical treatment within the counterion condensation theory, Biomacromolecules 7 (2006).
[24] G. Paradossi, E. Chiessi, M. Venanzi, B. Pispisa, A. Palleschi, Branched-chain analogues of linear polysaccharides: a spectroscopic and conformational investigation of chitosan derivatives, Int. J. Biol. Macromol. 14 (1992) 73–80.
[25] I. Geremia, M. Borgogna, A. Travan, E. Marsich, S. Paoletti, I. Donati, Determination of the composition for binary mixtures of polyanions: the case of mixed solutions of alginate and hyaluronan, Biomacromolecules 15 (2014) 1069–1073.
[26] C. Bustamante, I. Tinoco, M.F. Maestre, Circular differential scattering can be an important part of the circular dichroism of macromolecules, Proc. Natl. Acad. Sci. U. S. A. 80 (1983) 3568–3572.
[27] S.P. Strand, K. Tømmeraas, K.M. Vårum, K. Østgaard, Electrophoretic light scattering studies of chitosans with different degrees of N −acetylation, Biomacromolecules 2 (2001) 1310–1314.
[28] P. Riello, M. Mattiazzi, J.S. Pedersen, A. Benedetti, Time-resolved in situ small-angle X-ray scattering study of silica particle formation in nonionic water-in-oil microemulsions, Langmuir 24 (2008) 5225–5228.
[29] V.S. Murthy, R.K. Rana, M.S. Wong, Nanoparticle-assembled capsule synthesis: formation of colloidal polyamine-salt intermediates, J. Phys. Chem. B. 110 (2006) 25619–25627.
[30] G. Turco, I. Donati, M. Grassi, G. Marchioli, R. Lapasin, S. Paoletti, Mechanical spectroscopy and relaxometry on alginate hydrogels: a comparative analysis for structural characterization and network mesh size determination, Biomacromolecules 12 (2011) 1272–1282.
[31] M. Grassi, R. Farra, S.M. Fiorentino, G. Grassi, B. Dapas, Hydrogel mesh size evaluation, in: M. Pietro, A. Franco, C. Tommasina (Eds.), Polysacch. Hydrogels Charact. Biomed. Appl., Pan Stanford, 2015, pp. 139–165.
[32] I. Donati, S. Holtan, Y.A. Mørch, M. Borgogna, M. Dentini, G. Skjåk-Braek, New hypothesis on the role of alternating sequences in calcium-alginate gels, Biomacromolecules 6 (2005) 1031–1040.
[33] C. Löfgren, S. Guillotin, A.-M. Hermansson, Microstructure and kinetic rheological behavior of amidated and nonamidated LM pectin gels, Biomacromolecules 7 (2006) 114–121.
[34] E. Schuster, J. Eckardt, A.-M. Hermansson, A. Larsson, N. Lorén, A. Altskär, et al., Microstructural, mechanical and mass transport properties of isotropic and capillary alginate gels, Soft Matter 10 (2014) 357–366.
[35] F. Brun, A. Accardo, M. Marchini, F. Ortolani, G. Turco, S. Paoletti, Texture analysis of TEM micrographs of alginate gels for cell microencapsulation, Microsc. Res. Tech. 74 (2011) 58–66.
[36] G. Skjåk-Bræk, H. Grasdalen, O. Smidsrød, Inhomogeneous polysaccharide ionic gels, Carbohydr. Polym. 10 (1989) 31–54.